Pramāṇa, Vol. 24, No. 3, March 1985, pp. 443–456. © Printed in India.

# Change of confinement scale in nuclei and the EMC effect

SOURENDU GUPTA
Tata Institute of Fundamental Research, Bombay 400005, India

MS received 25 June 1984; revised 11 October 1984

**Abstract.** We study a model in which the confinement scale of quarks in a nucleus of mass $A$ changes as $A^{1/3}$. This explains the $A$ dependence of structure functions (EMC effect) as seen in muon, electron and antineutrino deep inelastic scattering from nuclear targets. We also investigate a prediction of this model—an $A$ dependence of the QCD scale parameter Λ.

**Keywords.** EMC effect; change of confinement scale in nuclei.

**PACS No.** 12·35; 13·60

## 1. Introduction

Since the time when scaling and the existence of point like constituents in the proton were observed in deep inelastic scattering (DIS) of electrons from protons, lepton DIS from nuclear targets has served as one of the principal testing grounds for QCD. It is assumed that the lepton-nucleus interaction takes place *via* a single photon (for $\mu$ and $e$, and $W$ or $Z$ in the case of the $\nu$ and $\bar{\nu}$) exchange (figure 1). One can then calculate the cross-sections for these processes as

$$\frac{d^2\sigma^{e\mu}}{dxdy} = \frac{8\pi\alpha^2 ME}{Q^4}[y^2xF_1(x) + (1-y)F_2(x)], \tag{1a}$$

$$\frac{d^2\sigma^{\nu\bar{\nu}}}{dxdy} = \frac{G^2 ME}{\pi}\left[y^2xF_1(x) + (1-y)F_2(x) \pm \left(y - \frac{y^2}{2}\right)xF_3(x)\right], \tag{1b}$$

where in the expression for the $\nu$, $\bar{\nu}$ cross-section, the positive sign for $F_3(x)$ occurs for $\nu$ and the negative for $\bar{\nu}$. Also $Q^2$ is the square of the 4-momentum of the exchanged photon, $\alpha$ is the fine structure constant, $G$ is the weak coupling constant, $E$ is the beam energy, $M$ the proton mass, $y = \nu/E$ where $\nu$ is the energy exchanged and $x$ $(= Q^2/2M\nu)$ is the Bjorken variable. In the infinite momentum frame (IMF), $x$ has the interpretation of the fraction of the target longitudinal momentum carried by the interacting quark.

Information on the quark substructure of the target is completely contained in the structure functions $F_1(x)$, $F_2(x)$, and $F_3(x)$. Of these, $F_1(x)$ and $F_2(x)$ are related by

$$(2xF_1(x) - F_2(x))/2xF_1(x) = R, \tag{2}$$

where $R$ is the ratio of the cross-sections for longitudinal and transverse photon scattering from a quark. For spin half quarks, in the parton model limit, $R = 0$ and we

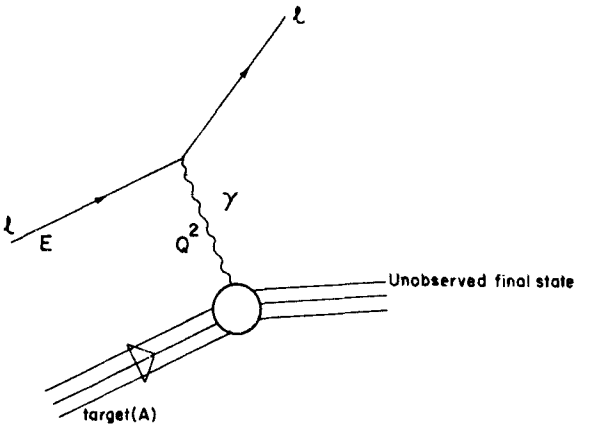


**Figure 1.** Deep inelastic lepton nucleus scattering with one exchanged photon.

get the Callan-Gross relation

$$F_2(x) = 2xF_1(x), \tag{3}$$

At finite $Q^2$, there are corrections to $R$ that give it a finite and non-vanishing value. In the scaling limit (*i.e.* at infinite $Q^2$), the structure functions depend only on $x$. At any finite $Q^2$ there are scaling violations that go roughly as $\ln Q^2$. This effect is predicted by QCD and the verification of this has been one of the prime motivations for DIS experiments.

The structure functions can be written in terms of quark (antiquark) densities for the target-$q_f(x)$ ($\bar{q}_f(x)$). These are the probability densities for finding quarks of longitudinal momentum fraction $x$ in the target.

$$F_2^{\mu,e}(x) = x\sum_f e_f^2[q_f(x)+\bar{q}_f(x)], \tag{4a}$$

$$F_2^{\nu,\bar{\nu}}(x) = x\sum_f [q_f(x)+\bar{q}_f(x)], \tag{4b}$$

$$F_3^{\nu,\bar{\nu}}(x) = \sum_f [q_f(x)-\bar{q}_f(x)] + 2[\bar{s}(x)-\bar{c}(x)]. \tag{4c}$$

The $\nu$ and $\bar{\nu}$ structure functions refer to isoscalar targets whereas the $\mu$ and $e$ structure functions are not so restricted. The corresponding isoscalar expressions for $F_2^{\mu,e}(x)$ can be obtained by averaging over the proton and neutron $F_2$s, remembering that the $u$ quark density in a proton equals the $d$ quark density in a neutron and vice versa. The quantitites $q_f(x)-\bar{q}_f(x)$ are known as the valence quark densities ($V(x)$) and $q_f(x) - V(x)$ and $\bar{q}_f$ are the sea quark densities. Throughout this paper, we assume a SU(3) flavour symmetric sea—*i.e.*, one with $\bar{c}(x) = 0$ and the $u$, $d$ and $s$ quark sea densities equal.

Muon DIS from deuterium and iron targets, performed recently by the European Muon Collaboration (EMC) has shown that $F_2^A(x)$ shows a marked variation with nuclear mass $A$ (Aubert *et al* 1983). These results have been verified for iron by the SLAC-MIT-Rochester group (Bodek *et al* 1983a, b) and also, more recently, by a series of

electron DIS experiments on different target nuclei done at SLAC (Arnold *et al* 1984). This $A$-dependence has been presented in the literature as the ratio

$$R^{A/d}(x) = F_2^A(x)/F_2^d(x), \tag{5}$$

where $F_2^d(x)$ is the structure function for deuterium. Previous expectations of $R^{A/d}(x)$ (Bodek and Ritchie 1981a, b; Frankfurt and Strikman 1981; Berlad *et al* 1980) are shown in figure 2 along with the EMC data points. It is apparent that the low and medium $x$ behaviour of the EMC data is the opposite of what was expected. However the rise in $R^{A/d}(x)$ at high $x$ predicted by these models has been confirmed by the SLAC experiments.

The strong enhancement of $R^{Fe/d}(x)$ at low $x$ has not been seen by the SLAC experiment. It was conjectured that this may be due to shadowing effects which are not present in the EMC data due to the high $Q^2$ range there. Neutrino DIS experiments on neon and deuterium targets done at BEBC also fail to show the low $x$ enhancement (Cooper *et al* 1984). However, all the experiments are consistent with each other for $x > 0{\cdot}2$.

Several models have been advanced to explain this so-called EMC effect. Excess pions, isobars and large clusters of quarks in nuclei have all been invoked to explain the ratio $R^{A/d}(x)$ (Llewellyn-Smith 1983; Ericson and Thomas 1983; Szwed 1983; West 1983; Cohen-Tannoudji and Navelet 1983). We propose a different approach based on the infrared regularization in QCD (Gupta *et al* 1983). A similar picture has also been considered by Jaffe (1983), Furmanski and Krzywicki (1984), Nachtmann and Pirner (1983), and Close *et al* (1984).

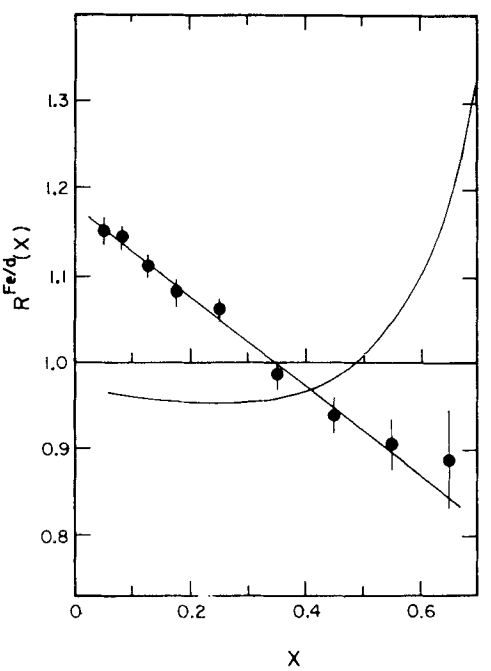


**Figure 2.** The ratio $R^{Fe/d}(x)$. The EMC data points and a straight line fit through them are shown. The rising curve is the prediction from the Bodek-Ritchie fermi smearing model.

## 2. The model

The EMC measurements have been carried out at high values of $Q^2$—ranging from about 9–170 GeV$^2$. The SLAC data are at lower values of $Q^2$, being restricted to less than 10 GeV$^2$. Nevertheless, the kinematic region of both sets of experiments is far above the nucleonic mass scale (1 GeV). It is then reasonable to assume that at these $Q^2$, the photonic probe does not "see" individual nucleons but only the quasi free quarks and gluons inside.

We therefore assume that the quarks and gluons (partons in an inclusive nomenclature) are no longer confined within individual nucleons but only within the nucleus as a whole. In that case, limits on the phase space of the partons are set not by the nucleonic size but by the size of the nucleus. Thus, the lower limit to the momenta of the partons is proportional to the inverse of the nuclear radius.

If, as usual we view the scattering event in the IMF, then the nucleus is flattened in the longitudinal direction to a disk. The cut-off then operates on the transverse momentum and is given by the inverse of the nuclear radius $r_0 A^{1/3}$. Hence

$$(p_t)_{\min} = bA^{1/3}, \tag{6}$$

where $b$ has a value between 100 and 200 MeV (being equal to $1/r_0$). The cut-off in $p_t$ decreases as we go to heavier nuclei. Hence partons inside nuclei have a larger phase space volume open to them than partons in a free nucleon. The evolution of quark densities is controlled by processes occurring inside a phase space volume bounded by $(p_t)_{\min}$ and $Q^2$. Hence, quark densities for one nucleus can be related to those for another by a simple change in the scale of $Q^2$. We recapitulate the well-known derivation of the Altarelli-Parisi equations (APE) (Altarelli and Parisi 1977) to show how these ideas can be incorporated into the standard QCD picture to yield the A-dependence of structure functions.

### 2.1 APE *and super* APE

In the naive parton model, a non-singlet structure function $F_{NS}$ is obtained by a sum over all flavours $f$ of the convolution of quark densities $V_f^0(y)$ in the target $A$ with the pointlike cross-section for quark photon scattering $\sigma_f$

$$F_{NS}(x) = \sum_f \int_x^1 dy/y \; V_f^0(x)\sigma_f(y), \tag{7a}$$

with

$$\sigma_f(y) = e_f^2 \delta(x/y - 1). \tag{7b}$$

The assumption is that the quark is on the mass shell and its momentum is a fraction $y$ of the target momentum. Also, the amplitude for the target-photon interaction can be factored into two incoherent subprocesses—the probability of finding a quark in the target and the pointlike quark photon cross-section. In this limit, there is no $Q^2$ dependence of the structure function.

In QCD, this factorization is still valid but the pointlike approximation to the cross-section can no longer be justified. The quark photon cross-section is obtained by contributions from a large set of diagrams. To first order in the coupling $\alpha$, one writes

$$F_{NS}(x, Q^2, A) = \sum_f \int_x^1 dy/y \; V_f^0(y) \left[e_f^2 \delta(x/y - 1) + \Delta\sigma_f(y, Q^2, A)\right], \tag{8}$$

where $\Delta\sigma_f(y, Q^2, A)$ is obtained by summing over diagrams of the type given in figure 3. An explicit computation with the real gluon emission diagram (figure 3a) yields

$$\Delta\sigma_f(y, Q^2, A) = e_f^2(\alpha/2\pi)\int dp_t^2/p_t^2\, P(y),$$

where $P(y)$ is independent of $Q^2$ and $A$. The $Q^2$ dependence of the cross-section comes purely from the upper limit to the integral. This is set by kinematics. There is a singularity at $p_t = 0$, *i.e.* for a real collinear gluon emission. In general an infrared regulator is placed at the lower limit of the integral to take care of the divergence. This reference mass is set in our model by $(p_t)_{\min}$. Hence the cross-section becomes

$$\Delta\sigma_f(y, Q^2, A) = e_f^2(\alpha/2\pi)tP(y), \tag{9}$$

where $t$ is defined as

$$t = \ln(Q^2A^{2/3}/b^2). \tag{10}$$

Now, in (8), the term in $t$ can be factored out and absorbed in a redefinition of the parton density, so that to order $\alpha$ we get

$$F_{NS}(x, Q^2, A) = \sum_f e_f^2 \int_x^1 dy/y\; V_f(y, Q^2, A)\delta(x/y - 1), \tag{11}$$

where

$$V_f(y, Q^2, A) = V_f^0(y) + (\alpha/2\pi)t\int_y^1 dz/z\; V_f^0(z)P(x/y)$$

The renormalization effects due to the virtual diagrams in figure 3 can be absorbed into $\alpha$ and the correct asymptotic form of the above equation can be written merely by changing $\alpha$ to the running coupling $\alpha(t)$ and hence writing

$$dV_f(x, t)/dt = (\alpha(t)/2\pi)\int_x^1 dy/y V_f(y, t)P(x/y). \tag{12}$$

This calculation can be repeated for the coupled singlet structure function $F_S(x)$ and gluon distribution $g(x)$. Putting in factors like $P(x/y)$ and integrating in the analogues of (12), we see that they consist of the three coupled equations (Abbot *et al* 1980)

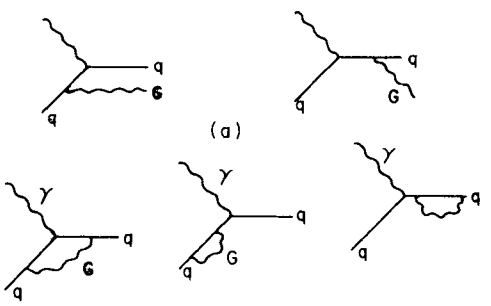


**Figure 3.** Processes contributing to $\Delta\sigma_f(y, Q^2, A)$. Figure 3a shows real gluon emission. The others are virtual processes contributing to the renormalization of the coupling.

$$\frac{\mathrm{d}}{\mathrm{d}t}F_{\mathrm{NS}}(x,t)=\frac{\alpha(t)}{3\pi}\left\{[3+4\ln(1-x)]F_{\mathrm{NS}}(x,t)+\int_x^1 \mathrm{d}z\left(\frac{2}{1-z}[(1+z^2)\ F_{\mathrm{NS}}(x,t)-2F_{\mathrm{NS}}(x,t)]\right)\right\}, \quad (13a)$$

$$\frac{\mathrm{d}}{\mathrm{d}t}F_S(x,t)=\frac{\alpha(t)}{3\pi}\left\{[3+4\ln(1-x)]F_S(x,t)+\int_x^1 \mathrm{d}z\left(\frac{2}{1-z}\left[(1+z^2)F_S\left(\frac{x}{z},t\right)-2F_S(x,t)\right]+\frac{9}{2}[z^2+(1-z)^2]g\left(\frac{x}{z},t\right)\right)\right\}, \quad (13b)$$

$$\frac{\mathrm{d}}{\mathrm{d}t}g(x,t)=\frac{3\alpha(t)}{\pi}\left\{\left[\frac{3}{4}-\ln(1-x)\right]g(x,t)+\int_x^1 \mathrm{d}z\left(\frac{zg\left(\frac{x}{z},t\right)-g(x,t)}{1-z}+\left[z(1-z)+\frac{1-z}{z}\right]g\left(\frac{x}{z},t\right)+\frac{2}{9}\left[\frac{1+(1-z)^2}{z}\right]F_S\left(\frac{x}{z},t\right)\right)\right\}. \quad (13c)$$

These equations look exactly like APES but contain an important new bit of information. Once the definition of the parton density is fixed for any given $Q^2$ and $A$, these quantities are automatically defined at all other $Q^2$ and $A$ by the super APE—equations (13).

The $Q^2$ and $A$ dependences of the parton densities are not independent but are related through the variable $t$ (equation (10)). As a result, in the context of this model, comparisons between structure functions of different nuclei are meaningful only after an $A$-dependent scaling of $Q^2$.

Since the momentum scale now depends on $A$, it is obvious that the extraction of the QCD scale parameter $\Lambda_{L0}$ from structure function data must be done only after the scaling of $Q^2$ has been done. Otherwise the observed scale parameters $\lambda^A_{L0}$ obtained from analyses of different target nuclei will be related by

$$\lambda^{A'}_{L0}=\lambda^{A}_{L0}(A/A')^{1/3}. \quad (14)$$

This is a consequence of the model open to direct experimental verification.

## 2.2 *Numerical method*

To test this model, it is necessary to have a parametrization for the quark and gluon densities and the value of $\Lambda_{L0}$. We have restricted ourselves to isoscalar nuclei. All the nuclei with $A < 40$ for which data are available happen to be isoscalar. Heavier nuclei have been corrected for neutron excess assuming for the EMC iron data (Aubert *et al* 1983)

$$F_2^n(x)=(1-0{\cdot}75x)F_2^p(x),$$

and for the SLAC iron, gold, and silver data (Arnold *et al* 1984)

$$F_2^n(x) = (1-0{\cdot}8x)F_2^p(x).$$

The structure function for an isoscalar nucleus then consists of only a singlet part and is written in the form

$$F_2(x) = 5/18\ F_s(x).$$

We then gain the computational advantage of having to work with only (13b) and (13c) instead of all three.

We parametrize $F_s(x)$ and the gluon distribution $g(x)$ for deuterium at $Q^2 = 20\,\text{GeV}^2$ as (Abbott *et al* 1980)

$$F_s(x) = C_1(1+C_2x)\,(1-x)^{C_3}, \tag{15a}$$

$$xg(x) = A_g(1-x)^{\alpha_g}. \tag{15b}$$

The momentum sum rule gives one constraint equation among these five parameters and is used to fix $A_g$ in terms of the other four. The four free parameters are varied along with $\Lambda_{LO}$ and used with the APE to give the best possible fit to the EMC data on $F_2^d(x)$. The results of this fit are given in table 1.

Apart from these singlet functions, we need the parametrization for the sea and valence quarks separately. Since we deal only with isoscalar nuclei, we do not need separate $u$ and $d$ quark densities but only one for $u+d$. We parametrize the valence and sea quark and gluon distribution for deuterium at $Q^2 = 20\,\text{GeV}^2$ as

$$xV(x) = A_v x^{\alpha_v}(1-x)^{\beta_v}, \tag{16a}$$

$$xS(x) = A_s(1-x)^{\beta_s}, \tag{16b}$$

$$xg(x) = A_g(1-x)^{\beta_g}. \tag{16c}$$

Again, the momentum sum rule is used to eliminate $A_g$. Moreover the parameter $A_v$ is fixed by sum rule constraint $\int_0^1 dx\ V(x) = 3$. Hence only five parameters are left free. The same data set as before is used to find the best values of these five parameters and $\Lambda_{LO}$. The results are displayed in table 1.

Having obtained these parametrization and the value of $\Lambda_{LO}$, the structure function $F_2^A(x)$ for any other nucleus and the EMC ratio—$R^{A/d}(x)$ can now be obtained using super APE as predictions based on this model. We present these and a comparison with experiments in § 3.

**Table 1.** Results of the 2 fits to the EMC data on $F_2^d(x)$. The four parameter fit has a $\chi^2/\text{DOF} = 62/47$ and the five parameter fit has $\chi^2/\text{DOF} = 63/46$.

| Four parameter fit | Five parameter fit |
|---|---|
| $c_1 = 0{\cdot}65 \pm 0{\cdot}02$ | $\alpha_v = 0{\cdot}53 \pm 0{\cdot}02$ |
| $c_2 = 2{\cdot}7\ \pm 0{\cdot}4$ | $\beta_v = 3{\cdot}26 \pm 0{\cdot}08$ |
| $c_3 = 3{\cdot}45 \pm 0{\cdot}09$ | $A_s = 0{\cdot}147 \pm 0{\cdot}009$ |
| $\alpha_g = 4 \pm 5$ | $\beta_s = 6{\cdot}6\ \pm 0{\cdot}2$ |
| | $\beta_g = 3 \pm 8$ |
| $\Lambda_{LO} = 96^{+77}_{-59}$ | $\Lambda_{LO} = 101^{+73}_{-77}$ |

## 3. Results using super APE

Using the parametrization for $F_s(x)$ and $g(x)$ for deuterium (equations (15)) with the values of the parameters given in table 1, we used super APE to compute $F_2^{Fe}(x)$. This prediction is, of course, dependent on the $\Lambda_{LO}$ value used. Varying $\Lambda_{LO}$ over the range of values allowed by the EMC deuterium data, we get the range of values for $F_2^{Fe}(x)$ that lie within the shaded band in figure 4. The EMC data on $F_2^{Fe}(x)$ are shown for comparison. Varying the other parameters over the range specified in table 1 does not change the structure function noticeably.

There is a clear systematic difference between the model prediction and the data for $x < 0{\cdot}3$. The model consistently underestimates $F_2^{Fe}(x)$ at low $x$. As a consequence, the low $x$ enhancement in $R^{Fe/d}(x)$ is absent. However at $x > 0{\cdot}3$, $F_2^{Fe}(x)$ agrees very well with the data. With a lower $x$-cut of 0·35 on the EMC data, the $\chi^2$ for a fit using super APE turns out to be 108·5 for 46 degrees of freedom. This is to be compared with an independent QCD fit to the same data set which yields a $\chi^2$ of 107·1 for 58 degrees of freedom. Hence, in this region super APE compares well with APE.

The SLAC data do not show the very strong enhancement in $R^{Fe/d}(x)$ at low $x$ which is the most noticeable feature of the EMC data. On the other hand they show $R^{A/d}(x)$ very close to 1 for very low $x$, increasing to a maximum at about $x = 0{\cdot}15$ and then falling off till $x = 0{\cdot}6$. This is the behaviour we see in our predictions of $R^{Fe/d}(x)$. The predicted values along with the data are given in figure 5. Similarly, our predictions for $R^{A/d}(x)$ agree well with the SLAC data for all the nuclei.

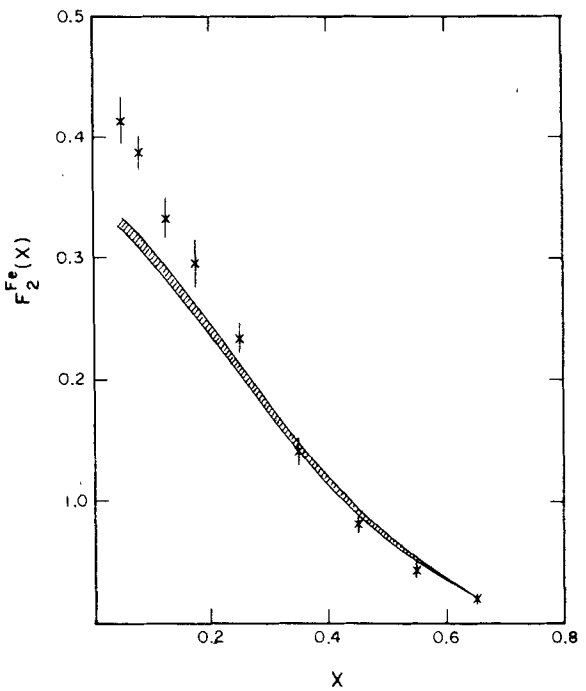


**Figure 4.** $F_2^{Fe}(x)$ computed in our model lies within the shaded band. The data points are the $Q^2$ averaged data from the EMC measurement of $F_2^{Fe}(x)$. The computed values have also been averaged over $Q^2$.

A further point to be noted is the $Q^2$ dependence of $R^{A/d}(x)$. Both the SLAC and EMC experiments show very little $Q^2$ variation of the ratio. A computation using super APE and $\Lambda_{LO} = 200$ MeV shows that the maximum variation in $R^{A/d}(x)$ over the range of $Q^2$ from 20–200 GeV$^2$ is about 7%. The $A$ and $x$ dependence of the $Q^2$ variation as calculated in this model is given in table 2. It is seen that the variation grows more marked with increasing $A$.

The prediction of the apparent $A$-dependence of $\Lambda_{LO}$ has been tested by making an independent QCD fit to the EMC data on $F_2^{Fe}(x)$ and extracting $\lambda_{LO}^{Fe}$. According to (14), we should expect the ratio $\lambda_{LO}^{Fe}/\lambda_{LO}^{d}$ to be 0·329. The computed values are given in table 3 for

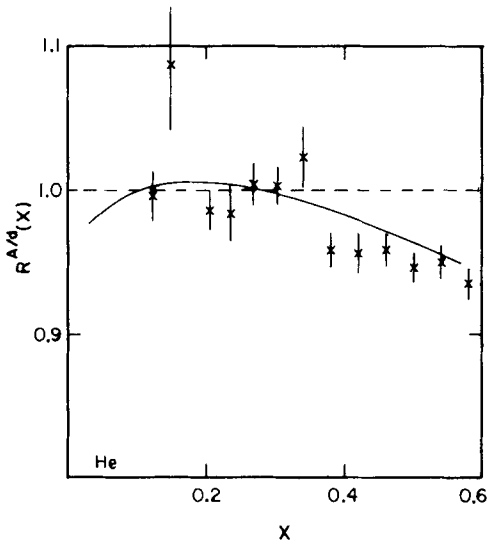


[a]

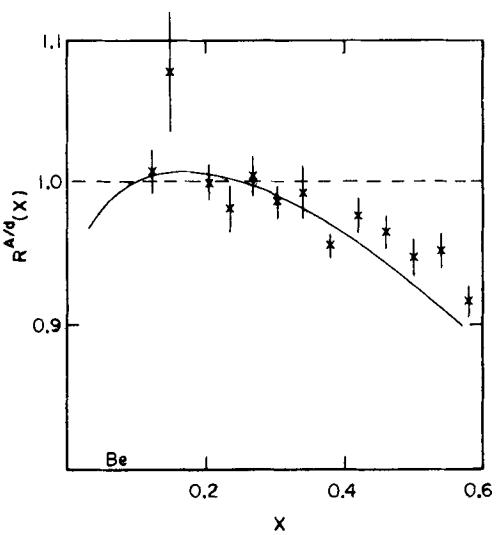


[b]

**Figures 5 a & b.**

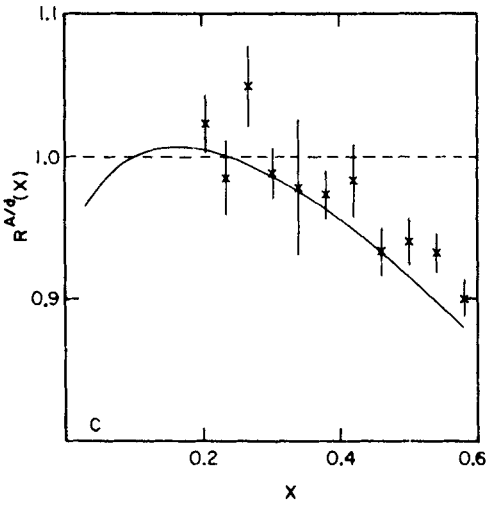


[c]

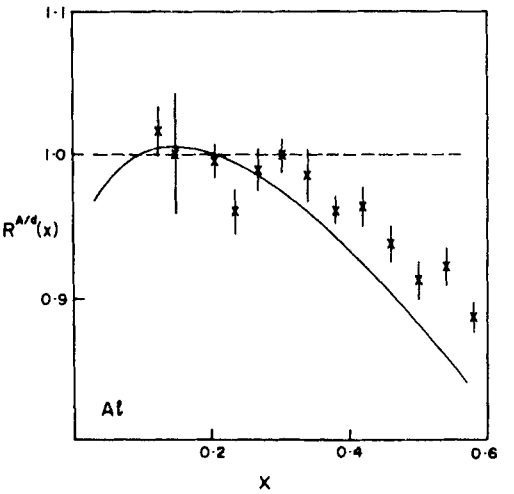


[d]

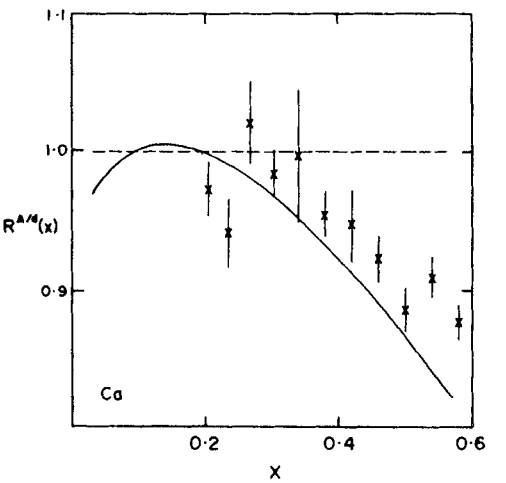


[e]

**Figures 5 c, d & e.**

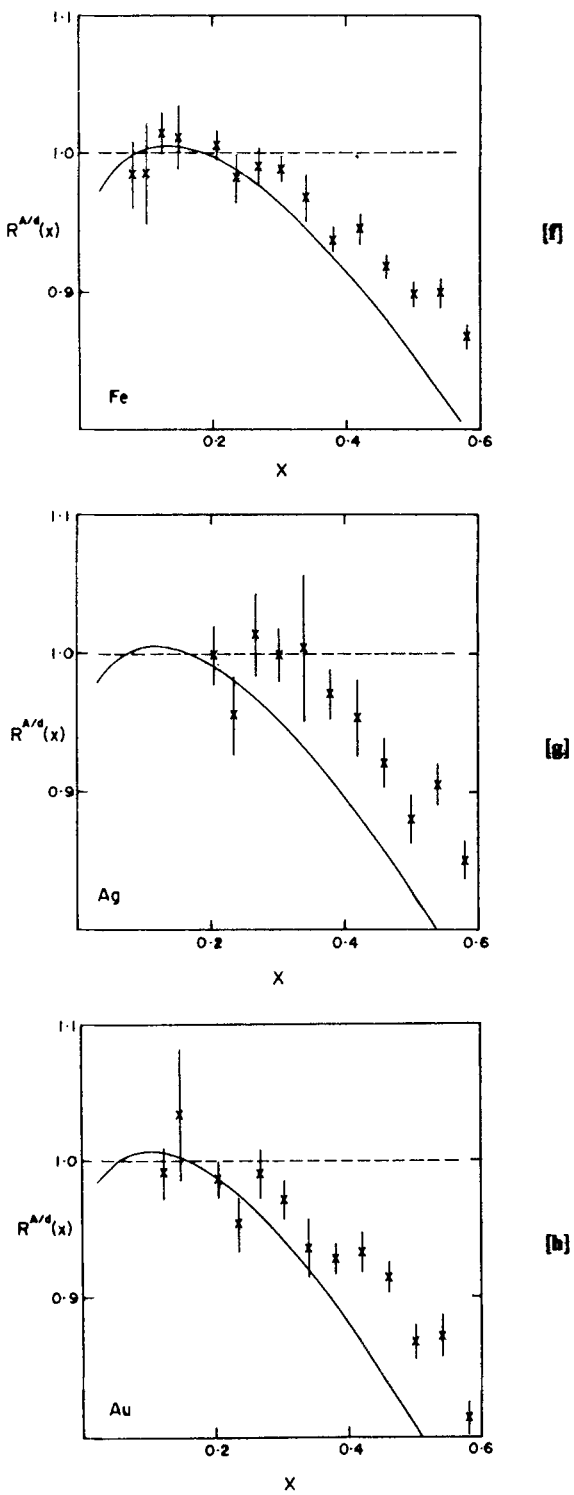


**Figure 5.** $R^{A/d}(x)$ for **a.** helium, **b.** beryllium, **c.** carbon, **d.** aluminium, **e.** calcium, **f.** iron, **g.** silver, and **h.** gold.

**Table 2.** The $Q^2$ variations of $R^{A/d}(x)$. The table shows the percentage change in $R^{A/d}(x)$ in going from $Q^2 = 20$–$200\,\text{GeV}^2$ for different $x$ and $A$.

| $A/x$ | 0·03 | 0·09 | 0·15 | 0·30 | 0·45 | 0·57 |
|---|---|---|---|---|---|---|
| 20 | 6·77 | 1·31 | −0·99 | −2·07 | −0·03 | 2·69 |
| 40 | 7·53 | 1·54 | −1·00 | −2·24 | −0·04 | 3·03 |
| 60 | 7·86 | 1·64 | −0·99 | −2·30 | −0·03 | 3·20 |
| 80 | 8·04 | 1·70 | −0·98 | −2·33 | −0·01 | 3·37 |
| 100 | 8·17 | 1·74 | −0·98 | −2·35 | 0·00 | 3·39 |

**Table 3.** The ratio $\lambda^{Fe}_{L0}/\lambda^{d}_{L0}$ for different $x$ cuts on the data. In all cases the ratio is close to the expected value of 0·33 although the errors are large.

| $x$ cut | $\lambda^{d}_{L0}$(MeV) | $\lambda^{Fe}_{L0}$(MeV) | $\lambda^{Fe}_{L0}/\lambda^{d}_{L0}$ |
|---|---|---|---|
| 0·35 | $277^{+158}_{-130}$ | $93^{+82}_{-57}$ | $0{\cdot}34^{+0{\cdot}36}_{-0{\cdot}26}$ |
| 0·45 | $344^{+87}_{-87}$ | $167^{+136}_{-93}$ | $0{\cdot}49^{+0{\cdot}42}_{-0{\cdot}30}$ |
| 0·55 | $774^{+367}_{-368}$ | $276^{+219}_{-169}$ | $0{\cdot}36^{+0{\cdot}33}_{-0{\cdot}28}$ |

several different lower $x$-cuts on the data. The central values are seen to be close to 0·329. However, the data do not fix either $\lambda^{Fe}_{L0}$ or $\lambda^{d}_{L0}$ well enough for us to make a very definite statement.

We have also calculated the ratio $\sigma^{\bar{\nu}}(\text{Ne})/\sigma^{\bar{\nu}}(d)$ in our model. The cross-sections have been integrated over $y$ for a comparison with the BEBC data on the ratio. This is shown in figure 6. Unfortunately, neutrino experiments suffer from a low event rate as compared

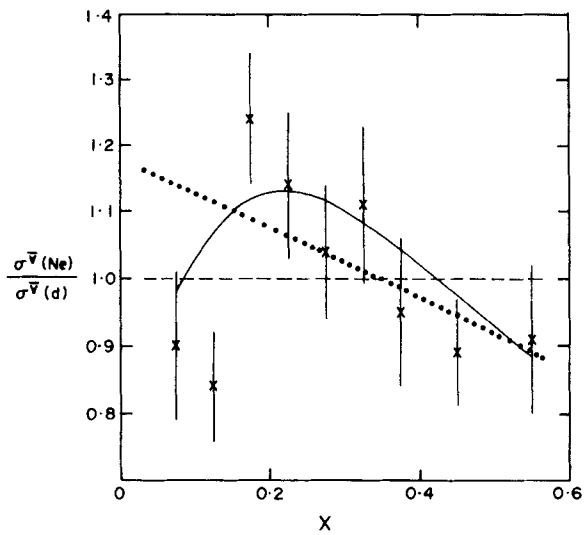


**Figure 6.** BEBC measurement of the ratio of $\bar{\nu}$ DIS cross-sections from neon and deuterium targets are compared to our computations (full line). The best fit to the EMC data on $R^{Fe/d}(x)$ is given by the dotted line. The dashed line is the expectation for no $A$-dependence.

to the muon or electron events, as a result of which the statistical errors are much larger. Nevertheless, fits to the BEBC data using super APE are much better ($\chi^2/d\,of = 12{\cdot}2/9$) than the other models considered by the BEBC—for example the best fit line from EMC ($\chi^2/d\,of = 21{\cdot}9/9$) or the no nuclear effect line ($\chi^2/d\,of = 16{\cdot}0/9$). We have used the data cut at $Q^2 = 4{\cdot}5\,\text{GeV}^2$. This has an average $Q^2$ of about $10\,\text{GeV}^2$. We have also calculated the $Q^2$ variation of this ratio and compared it with the BEBC data in table 4. Again, within the range of experimental errors, our computations seem consistent with the data.

We have used super APE to evolve the valence and sea quarks and the gluon distributions to different values of $A$. The momentum fraction carried by each species in different nuclei are shown in figure 7. It is seen that momentum is transferrred from valence quarks to sea quarks and gluons as we go to heavier nuclei. This manifests itself as the dip in the ratio $R^{A/d}(x)$ at high $x$. It is also interesting to note that in heavy nuclei gluons gain momentum at the expense of quarks. This means that the low $x$ enhancement of $R^{A/d}(x)$ does not balance out the high $x$ depletion.

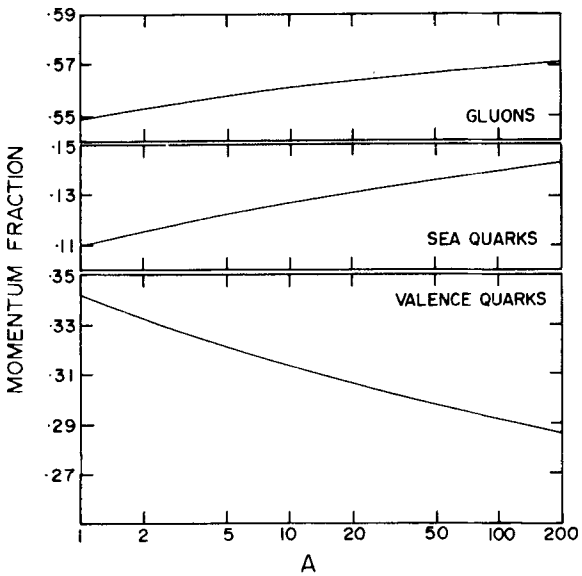


**Figure 7.** $A$-dependence of the momentum fraction carried by valence and sea quarks and gluons in a target.

**Table 4.** The $Q^2$ variation of the ratio of $\bar{\nu}$ cross-sections for a target of mass $A$ to a deuterium target. The table shows the percentage variation in the ratio in going from $Q^2 = 2$–$20\,\text{GeV}^2$ for different $x$ and $A$.

| $A/X$ | 0·03 | 0·09 | 0·15 | 0·30 | 0·45 | 0·57 |
|---|---|---|---|---|---|---|
| 20 | 5·77 | 4·50 | 3·70 | 1·07 | −3·46 | −6·24 |
| 40 | 7·25 | 5·55 | 4·47 | 1·13 | −3·59 | −7·90 |
| 60 | 8·04 | 6·10 | 4·87 | 1·14 | −4·10 | −8·83 |
| 80 | 8·58 | 6·47 | 5·14 | 1·14 | −4·45 | −9·47 |
| 100 | 8·98 | 6·75 | 5·34 | 1·11 | −4·72 | −9·96 |

## 4. Conclusions

The model we have presented here allows us to understand the EMC effect in terms of the normal QCD evolution. As such, it furnishes us with a framework for computing the $A$-dependence of structure functions without the addition of further parameters to be fitted to experimental data.

The model predicts an apparent $A$-dependence of the QCD scale parameter $\Lambda_{LO}$—an effect that is probably seen in the data. A further check on this is possible only with high quality DIS data on a series of nuclei.

Predictions for $F_2^{Fe}(x)$ agree with the EMC data at $x > 0{\cdot}35$ but deviate systematically from the measured values at lower $x$. This is also manifested in our computation of $R^{Fe/d}(x)$—which agrees with the EMC data at high $x$ but deviates at lower $x$. However, the model predictions fit the SLAC data on $R^{A/d}(x)$ for a large number of nuclei. These data are at $\langle Q^2 \rangle = 5\,\text{GeV}^2$ whereas the EMC data are at $\langle Q^2 \rangle = 40\,\text{GeV}^2$. The $Q^2$ dependence—or the lack of it—of $R^{A/d}(x)$ is well reproduced in our model.

Further checks come from $\bar{\nu}$ DIS experimental data with neon targets from the BEBC group. However, the errors in these data are so large that not much more than trends can be analyzed. Nevertheless, as far as it is possible to conclude anything from this data, it seems to fit our model—both in the $x$ and $Q^2$ dependence of the ratio.

The tests we have already performed can be made more stringent by high quality data on a large number of nuclei. As far as the available data are concerned the model explains the $A$-dependence of structure functions in the range $0{\cdot}3 < x < 0{\cdot}7$ extremely well.

## Acknowledgements

The author is grateful to Prof. B. Banerjee and Dr. R. M. Godbole for discussions.

## References

Abbot L F, Atwood W B and Barnett R M 1980 *Phys. Rev.* **D22** 582
Altarelli G and Parisi G 1977 *Nucl. Phys.* **B126** 298
Arnold R G *et al* 1984 *Phys. Rev. Lett.* **52** 727
Aubert J J *et al* 1983 *Phys. Lett.* **B123** 275
Berlad G , Dar A and Eilam G 1980 *Phys. Rev.* **D22** 1547
Bodek A *et al* 1983a *Phys. Rev. Lett.* **50** 1431
Bodek A *et al* 1983b *Phys. Rev. Lett.* **51** 534
Bodek A and Ritchie J L 1981a *Phys. Rev.* **D23** 1070
Bodek A and Ritchie J L 1981b *Phys. Rev.* **D24** 1400
Close F E, Roberts R G and Ross G G 1983 *Phys. Lett.* **B129** 346
Cohen-Tannoudji G and Navelet H 1983 CEN Saclay preprint S Ph T-83-97
Cooper A M *et al* 1984 *Phys. Lett.* **B141** 133
Ericson M and Thomas A W 1983 *Phys. Lett.* **B128** 112
Frankfurt L L and Strikman M I 1981 *Nucl. Phys.* **B181** 22
Furmanski W and Krzywicki A 1984 *Z. Phys.* **C22** 391
Gupta S, Banerjee B and Godbole R M 1983 TIFR Preprint TIFR/TH/84-8
Jaffe R L 1983 *Phys. Rev. Lett.* **50** 228
Llewellyn-Smith C M 1983 *Phys. Lett.* **B128** 107
Nachtmann D and Pirner H J 1984 *Z. Phys.* **C21** 277
Szwed J 1983 *Phys. Lett.* **B128** 228
West G B 1983 Los Alamos Preprint LA-UR-83-2504